UDK/*UDC*: 502.3:504.7(497.521. 2)
Izvirni znanstveni članek – *Original scientific paper*
DOI: 10.15292/acta.hydro.2023.10

Prejeto/*Received:* 25.02.2024
Sprejeto/*Accepted:* 19.03.2024
Objavljeno na spletu/*Published online:* 31.05.2024

DIFFERENT DEVELOPMENT OF GLOBAL WARMING (GW) AND URBAN HEAT ISLAND (UHI) IN THE CITY OF ZAGREB

RAZLIČEN RAZVOJ GLOBALNEGA SEGREVANJA (GS) IN MESTNEGA TOPLOTNEGA OTOKA (UHI) V MESTU ZAGREB

Ognjen Bonacci [1], Adrijana Vrsalović [1], Tanja Roje-Bonacci [1]

[1] Faculty of Civil Engineering, Architecture and Geodesy, Split University, Matice Hrvatske 15, 21000 Split; obonacci@gradst.hr (O.B.), bonacci@gradst.hr (T.R.B.)

Abstract

The analysis examines various impacts of global warming (GW) and urban heat island (UHI) effects at four meteorological stations in and around Zagreb, Croatia, spanning from 1981 to 2021. The goal was to determine the intensity and causes of the different warming tendencies and behaviour of air temperature variations observed in various parts of Zagreb. Data from four meteorological stations were analysed: Grič (GR) – a hill within the city area, Maksimir (MA) – an urbanized suburban area, Pleso (PL) – a suburban area unaffected by intense urbanization (airport), and Puntijarka (PU) – atop of Mt. Medvednica. Various statistical methods were applied to analyse trends and variations in annual, monthly, and daily air temperature indices (ATI), including linear regression, the Mann–Kendall test, the day-to-day variability method (DTD), and diurnal air temperature range (DTR) method. All stations showed increasing trends in all ATI. At the PU station, the trend is solely due to GW; at others, both UHI and GW contribute. The MA station exhibits the most pronounced UHI. DTD variability decreases at all stations. GR sees an increasing DTR trend, while PU's trend is decreasing. No DTR trends were observed at the other two stations. Overall, ATI variations are similar, but each location's behaviour differs due to its unique local environment.

Keywords: global warming (GW), urban heat island (UHI), air temperature trend, day-to-day air temperature variability (DTD), diurnal air temperature range (DTR), Zagreb City

Izvleček

Analiza preučuje različne vplive učinkov globalnega segrevanja (GW) in mestnega toplotnega otoka (UHI) na štirih meteoroloških postajah v Zagrebu in okolici (Hrvaška) v obdobju od leta 1981 do 2021. Cilj je ugotoviti intenzivnost in vzroke za različne težnje segrevanja in obnašanje spreminjanja temperature zraka v različnih delih mestnega območja Zagreba. Analizirani so podatki s štirih meteoroloških postaj: Grič (GR) – mestno središče, Maksimir (MA) – urbanizirano primestno območje, Pleso (PL) – primestno območje, neprizadeto zaradi intenzivne urbanizacije (letališče), in Puntijarka (PU) – na vrhu planine Medvednica. Za analizo trendov

[1] Stik / *Correspondence*: avrsalovic@gradst.hr

in sprememb letnih, mesečnih in dnevnih indeksov temperature zraka (ATI) so bile uporabljene različne statistične metode, vključno z linearno regresijo, Mann-Kendallovim testom, metodo dnevne variabilnosti (DTD) in razponom dnevne temperature zraka (DTR). Vse postaje so pokazale naraščajoče trende pri vseh ATI. Na postaji PU je trend izključno zaradi GW; pri drugih prispevata tako UHI kot GW. Postaja MA kaže najbolj izrazit UHI. Spremenljivost DTD se zmanjša na vseh postajah. Pri postaji GR je naraščajoči trend DTR, medtem ko se ta trend pri postaji PU zmanjšuje. Na drugih dveh postajah ni bilo opaziti nobenih trendov. Na splošno je spreminjanje ATI podobno, a obnašanje se na vsaki lokaciji razlikuje zaradi edinstvenega lokalnega okolja.

Ključne besede: globalno segrevanje (GW), mestni toplotni otok (UHI), trend temperature zraka, spremenljivost dnevne temperature zraka (DTD), razpon dnevne temperature zraka (DTR), mesto Zagreb.

1. Introduction

The phenomenon of urban heat island (UHI) refers to an urban or metropolitan area that is significantly warmer than its surroundings (Nuruzzaman, 2015). It is explained by the fact that intensive human development concentrated in relatively small urban areas lead to much warmer ambient temperatures than in nearby larger non-urbanized territory. UHI occurs simultaneously with the global warming (GW) process, which refers to the unusually rapid increase in the overall temperature of the Earth's atmosphere (Stocker et al., 2013). GW and UHI effects co-exist in rapidly developed towns.

The overwhelming majority, nearly without exception, of the scientific community believes that the average temperature of the Earth's atmosphere is rising due to the increased amount of greenhouse gases produced by human activities (L. El Zein, 2015; Raupach and Fraser, 2011). It is of crucial practical as well as theoretical importance to understand precisely the influence of UHI on increases in local air temperature, which are generally governed by GW. A better explanation of future UHI and GW development can effectively contribute to the sustainable development of urban agglomerations.

The uncontrolled increase of UHIs will cause very negative consequences on the environment, ecosystem, social and health processes, as well as adverse economic impacts. UHIs can significantly affect water availability in urban areas. The elevated temperatures within UHIs lead to increased rates of evaporation from water bodies, soils, and vegetation (Santamouris, 2014). This accelerated evaporation reduces the overall water content in urban environments, diminishing water availability for various purposes such as irrigation, drinking water, and industrial use. Additionally, UHIs can alter precipitation patterns, often resulting in decreased rainfall and prolonged dry periods in urban areas (Oke, 1982). These changes in precipitation further exacerbate water scarcity issues in cities.

UHIs are the main adverse effect of urbanization (Antoszewski et al., 2022). Addressing UHI challenges requires urgent and efficient measures. Because the increase of UHI negatively affects economic productivity and public health, He et al. (2022) suggest population migration out of the extreme urban heat areas in China. Based on the above facts, Gonzalez-Trevizo et al. (2021) emphasize that scientific research on UHI and urban overheating poses challenges for societies in terms of risk management, energy demands, and mitigation strategies for improving urban environmental quality and reducing pollution.

The development of the UHI process depends on the interaction of numerous natural and anthropogenic factors, which are very different for each urban area. There are many reasons why UHIs contribute to ambient air temperatures increasing in urban areas. The most important are: (1) industrial activities (Li et al., 2011; Meng et al., 2022); (2) traffic (Louiza et al., 2015); (3) heating during the winter period (Giridharan and Kolokotroni, 2009); (4) urban form (Cekinir et al., 2022; Clay et al., 2016; Lemoine-Rodríguez et al., 2022; Milošević et al., 2022); (5) cooling due to use of air conditioners during the summer period (de Munck et al., 2013; Kolokotroni et al., 2006); (6) pavement (Deluka-Tibljaš et al., 2012). The last of these reasons has drastically increased the UHI effect in Croatian towns in recent decades.

Using the Weather Research and Forecasting model in three differently sized Japanese cities, Takebayashi & Senoo (2018) concluded that the spatial average air temperature in urban areas rises with the expansion of the urban center's size. This emphasizes the substantial influence of urban expansion in intensifying the UHI effect.

Urban form centrality has a strong influence on its thermal environment. Based on the analyses made in Chinese megacities, Lu et al. (2022) stressed that concentric urban form leads to a monocentric urban thermal environment. They consider that restraining urban spread could alleviate UHI effects and thus improve urban thermal environments.

Analyzing the relationship between urban form and UHI intensity along the urban development gradients of 150 urban areas in the Jing-Jin-Ji region of China in 2000, 2005, 2010, and 2015, Liang et al. (2020) found that urban continuity, complexity, population density, and Normalized Difference Vegetation Index had a greater influence, while urban elongation, night-time light index, and tree cover had a lesser influence.

Another reason UHIs are more intense in urban areas is that wind speeds are lower due to wind sheltering. Allegrini & Carmeliet (2018) simulated the impact of new buildings on the local urban microclimate for a building site in Zurich, Switzerland, and found that the formation of local hot spots depends strongly on building geometry, construction materials, and wind directions and speeds. Using 64 airport climate records across Canada, Gough & Leung (2022) assessed the nature of the local environment. By analyzing peri-urban thermal metrics and populations, they concluded that airports have a peri-urban climate regardless of the size of the local population or the degree of urbanization. This result provides evidence for the existence of distinct local climates around airports, consistent with peri-urban characteristics.

Local landscape characteristics, geological conditions, environmental factors, land surface characteristics, vegetation cover, and the vicinity of a river or a lake, etc. may have a strong influence on the attenuation or intensifications of UHI effects at neighboring locations. Peterson (2003) considers that all analyses of the impact of UHIs on in-situ temperature observations suffer from inhomogeneity or biases in the data, which make UHI analyses difficult and may lead to erroneous conclusions. He concluded that a variety of adjustments were applied to the data in order to remove the biases caused by differences in elevation, latitude, time of observation, instrumentation, and nonstandard siting.

The analysis of UHI should be considered an exceptionally important topic with many unsolved questions (Bonacci et al., 2018). The goal of the study this paper describes was to better understand the impact of various urbanization developments on air temperature increases. It is crucial to distinguish the UHI effect from the existing GW effect, a task that poses significant complexity and challenges. Some methods to assess urban influence involve comparing trends between urban stations and rural stations, while others use indirect criteria, such as comparing trends of minimum temperature values from urban meteorological stations under calm conditions with those under windy conditions, as UHI increases under low wind speed (Alcoforado and Andrade, 2008).

Using three different approaches (trend analyses, day-to-day variability method, and diurnal air temperature range method), this paper analyses the changes in the relationship between time series of annual, monthly, and daily air temperatures indices (ATI) at four meteorological stations located in various parts of Zagreb. The paper attempts to determine the extent to which the warming trend observed at the different urban locations is caused by the UHI.

2. Materials and methods

2.1 Characteristic of four analyzed stations

Table 1 contains the latitude, longitude, and elevation of the following four climate stations: (1) Grič (GR); (2) Maksimir (MA); (3) Pleso (PL); (4) Puntijarka (PU). Figure 1 shows the locations, distances, and photos of the meteorological stations, from which one can get a first impression of the characteristics of their locations. Figure 1 also presents Zagreb's urban development over the past more than 150 years, from 1857 to the present.

During this time Zagreb's urban area grew from less than 100 km^2 up to 1700 km^2, and the population increased from 5000 to 769,944 inhabitants (according to the 2021 census).

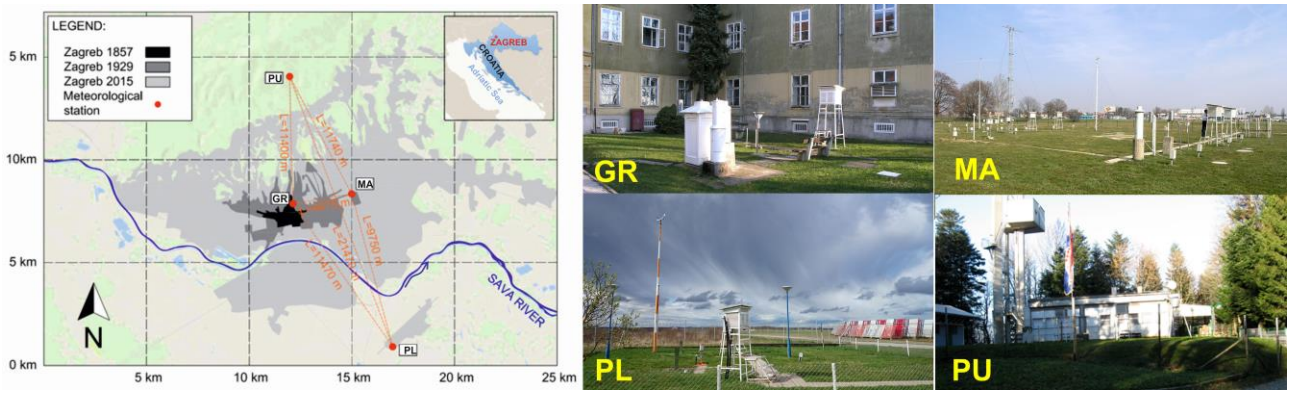

***Figure 1**: Map and photos of four analyzed climate stations.*

***Slika 1**: Karta in fotografije štirih analiziranih meteoroloških postaj.*

***Table 1**: List of analyzed climate stations with their latitude, longitude, and elevation.*

***Preglednica 1**: Seznam analiziranih meteoroloških postaj z njihovo zemljepisno širino, dolžino in nadmorsko višino.*

Station name	Latitude (N)	Longitude (E)	Elevation (m a.s.l.)
GRIČ (GR)	45° 48' 52"	15° 58' 19"	157
MAKSIMIR (MA)	45° 49' 19"	16° 02' 01"	123
PLESO (PL)	45° 43' 45"	16° 03' 14"	106
PUNTIJARKA (PU)	45° 54' 27"	15° 58' 06"	991

The intensely developed urban part of Zagreb is located on the north/left bank of the Sava River. It spreads on the slope of Mt. Medvednica, a massif stretching for 42 kilometers in a northeast-southwest direction, whose peak is 1035 m above sea level (m a.s.l.). Three (GR, MA, and PU) of the four analyzed climate stations are in this part of the city. The last climate station PL is located at the city airport in the new part of the city, called Novi Zagreb, on the south/right bank of the Sava River. Novi Zagreb began expanding in 1953. It is mostly residential, consisting of blocks of flats and tower blocks. In the northern part of the city, local topography played an important role in the formation and evolution of the UHI (Nitis et al., 2005); intensive urbanization strongly influences the natural wind patterns and thus UHI (Klaić et al., 2002).

None of the the stations or measurement instruments have ever been moved since their installation. The standard normal homogeneity test, Likso, (2003) shows that the air temperature's time series at analyzed climate stations are homogenous. Air temperature is measured on a thermometric screen, 2 m above the ground.

The Grič Observatory (GR) operates on a small hill downtown, located beneath the foothills of Mt. Medvednica. This location has been intensively exposed to UHI for a long time. The analyses of air temperature trends made by Bonacci and Roje-Bonacci (2018) showed that the minimum annual air temperatures began warming in 1970, mean annual air temperatures in 1988, and maximum annual air temperatures in 1998. In the second half of the 20th century, the increase in air temperature was accompanied by a statistically significant decrease in variability, observed in the series of

daily maximum temperatures and the difference between daily maximum and minimum temperatures (Bonacci et al., 2022).

The climate station MA is about 4 km east of the Zagreb City Centre. The local landscape in the broader area is predominantly flat. In recent decades, this part of the city has been influenced by intensive urbanization widely recognized as a new housing development built on a mix of former farmland and rural environment. Hectares of asphalt and roofs in recent decades have been built on the previous agricultural area (Bonacci et al., 2018).

The climate station PL is located at Zagreb's airport on a plain 10 km southeast of the Zagreb city Centre and 2.5 km south of the Sava River (Figure 1), near the suburban village of Pleso. From the photograph given in Figure 1, it can be seen the surrounding terrain is considerably flat and predominately covered by grasslands. Due to the airport's expansion and operation, other processes of urbanization in this area are less intensive. Because of the Sava River's vicinity and of shallow groundwater levels, this location recorded more days with fog than the wider Zagreb metropolitan area (Brzoja, 2012; Zoldoš and Jurkovic, 2016).

The PU climate station is positioned about 10 km north of Zagreb, near the top of Mt. Medvednica at an elevation of 991 m a.s.l., just 47 m below its peak. It is placed in an opening surrounded by a dense natural woodland, which can be seen in Figure 1. Its position is more than 600 m higher and 7 km laterally from the suburban area dotted with large houses on the mountain hill slope. Situated as it is atop a mountain, the PU station is sufficiently far away from Zagreb's urban area and thus cannot be influenced by UHI (Seletković et al., 2009). Because of this, it is realistic to assume that the air temperature monitored at the PU climate station is not influenced by UHI. Thus, its increasing air temperature trend can be explained by the GW effect only (Bonacci et al., 2018).

Nimac et al. (2021) examined changes in extreme air temperatures at the same four climate stations as we did in this paper. They concluded that changes in extreme temperatures were least pronounced in the mountains compared to the other urban stations. Their results suggest a potential increase in risk associated with warm events that were more pronounced during warm summer extremes.

Seletković et al. (2023) analyzed the UHI analysis for the city of Zagreb in 2013-2022 using Landsat-8 satellite imagery. They concluded that forested areas and other green parts of the urban infrastructure have the lowest temperatures, while built-up areas are the hottest points in cities. This conclusion underscores the importance of green urban infrastructure for resilient cities.

2.2 Methods used

The air temperature data used in this study were provided by the Croatian Meteorological and Hydrological Service (DHMZ). In this study, the minimum, mean, and maximum daily and annual air temperature, and mean monthly air temperatures for the period from 1 January 1981 to 31 December 2021 were analyzed. The method employed by the DHMZ calculates the mean daily air temperature $T_{mean,daily}$ using the following equation:

$$T_{mean,daily} = \frac{T_7 + T_{14} + (2 \cdot T_{21})}{4} \quad , \qquad (1)$$

where T_7, T_{14}, and T_{21} are the air temperature values measured at 7, 14, and 21 h (local time), respectively.

2.2.1 Trend analyses

The linear trend of all analyzed time series was calculated using linear regressions analyses. The linear regression equation is:

$$T = (a \cdot t) + b \quad , \qquad (2)$$

where T is the analyzed air temperature in year t, and a and b are linear regression calculated by the least-squares method. The coefficient a represents the slope of the regression line whose dimension is °C/time, which in this paper can be month or year. It is the indicator of the average intensity of the increasing or decreasing trends in the values of the analyzed time series. The coefficient of determination R^2 shows the strength and the direction of linear correlation between the time variable t and the analyzed monthly or annual air

temperature indices. Except for trend analyses, the coefficients of determination R^2 are used in the paper to measure how strong a relationship is between two variables. The absolute value of the coefficient of determination gives the relationship strength. The larger the number, the stronger the relationship.

To assess whether the time series have monotonic increasing or decreasing trends, the original non-parametric Mann–Kendall (M–K) test was used (Hussain and Mahmud, 2019). The null hypothesis is that there is no statistically significant monotonic trend within the analyzed time series, while the alternative hypothesis is that a statistically significant trend exists. As a criterion to accept the alternate hypothesis probability, $p<0.01$ is used.

2.2.2 DTD method of air temperature variability

The following equation is used to calculate the DTD variabilities in air temperatures (Gough, 2008; Gough and Hu, 2016; Gough and Shi, 2020; Moberg et al., 2000):

$$DTD = \sum |T_i - T_{i-1}|/(N-1) \quad (3)$$

where N denotes the number of included daily air temperature data, and *i* represents the day counter during the considered time.

The differences ΔDTD between the maximum daily air temperatures T_{max} ($DTDT_{max}$) and the minimum daily temperatures T_{min} ($DTDT_{min}$) is calculated using the following equation developed by Gough (2008):

$$\Delta DTD = DTDT_{max} - DTDT_{min} \quad (4)$$

The positive values of differences calculated by equation (4) indicate that daytime temperature variabilities are greater than nighttime ones, while the negative values of differences reveal that variabilities in the nighttime temperatures are greater than the daily ones. Tam et al. (2015) found that urban environments had considerably higher values compared to nearby rural locations.

2.2.3 DTR method

Daily diurnal temperature range (DTR) data was obtained by subtracting the daily minimum temperature from the daily maximum temperature at each station. DTR is an important meteorological indicator for the intensity of global climate change (Easterling et al., 1997; Karl et al., 1987, 1984; Vose et al., 2005). DTR describes the within-day temperature variability and reflects weather stability. It is defined as the difference between the daily maximum air temperature $T_{max,i}$ and the daily minimum air temperature $T_{min,i}$ for day i during the analyzed period (year, season, month, etc.):

$$DTR = \sum (T_{max,i} - T_{min,i})/N \quad , \quad (5)$$

where, i = {={1, 2, 3, …, ,…,N)} and N is the number of observations.

Analyzing DTR change in the continental US, Qu et al. (2014) found that fall and summer witnessed a significant decrease in DTR in all regions, while spring and winter have experienced much smaller decreases. To predict the change in DTR, Park and Joh (2005) used climate models to conclude that, as surface air temperature increases, the diurnal temperature range decreases, primarily due to a greater increase in nocturnal minimum temperatures relative to diurnal maximum temperatures.

3. Results

3.1 Trend of annual ATI

The annual analysis is a valuable tool for quantifying the overall warming trends resulting from the combined effects of global warming and urbanization. Table 2 represents the matrix with values of the average T_{av}, absolute minimum T_{min}, absolute maximum T_{max}, span S, slope of linear equation a, the coefficients of determination R^2, and the probability of the M-K test p, for the annual time series of temperature indices (mean, minimum, maximum) measured at four meteorological stations during the analyzed period 1981–2021. M–K p values $p<0.01$ are highlighted in red.

Table 2: *List of the average T_{av}, absolute minimum T_{min}, absolute maximum T_{max}, span S, the slope of linear equation a, the coefficients of determination R^2, and the probability of the M–K test p for the annual time series of temperature indices (mean, minimum, maximum) measured at four meteorological stations during the analyzed period 1981–2021. M–K p values p < 0.01 are highlighted in red.*

Preglednica 2: *Seznam povprečja, T_{av}, absolutnega minimuma, T_{min}, absolutnega maksimuma, T_{max}, razpona, S, naklona linearne enačbe, a, koeficientov determinacije, R^2, verjetnosti preskusa M–K, p, za letno časovno vrsto temperaturnih indeksov (povprečje, minimum, maksimum), izmerjeno na štirih meteoroloških postajah v analiziranem obdobju 1981–2021. M–K vrednosti p, p < 0,01, so označene rdeče.*

	GRIČ	MAKSIMIR	PLESO	PUNTIJARKA
T_{av} (ºC)	12.61	11.55	11.35	7.19
T_{min} (ºC)	-17.2	-22.6	-24.1	-20.8
T_{max} (ºC)	38.8	38.6	39.1	32.3
$S=T_{max}-T_{min}$ (ºC)	56.0	61.2	63.2	53.1
a_{mean}	0.0603	0.0652	0.0585	0.0535
R^2_{mean}	0.593	0.623	0.618	0.511
p_{mean}	**9.3E-08**	**7.0E-09**	**3.7E-08**	**5.9E-07**
a_{min}	0.0743	0.1065	0.1254	0.0597
R^2_{min}	0.089	0.109	0.129	0.074
p_{min}	0.099	0.064	0.017	0.101
a_{max}	0.0845	0.0717	0.0618	0.0558
R^2_{max}	0.300	0.197	0.138	0.117
p_{max}	**3.8E-04**	**3.5E-03**	0.028	0.057

Table 3: *List of the coefficients of determination R^2 between the characteristic annual (minimum, mean, maximum) air temperature time series of four analyzed stations during the 1981–2021 period.*

Preglednica 3: *Seznam koeficientov determinacije, R^2, med značilnimi letnimi (minimalnimi, srednjimi, maksimalnimi) časovnimi vrstami temperature zraka na štirih analiziranih postajah v obdobju 1981–2021.*

minimum	GRIČ	MAKSIMIR	PLESO	PUNTIJARKA
GRIČ	1	0.861	0.750	0.528
MAKSIMIR		1	0.931	0.530
PLESO			1	0.472
PUNTIJARKA				1
mean	GRIČ	MAKSIMIR	PLESO	PUNTIJARKA
GRIČ	1	0.978	0.974	0.951
MAKSIMIR		1	0.990	0.914
PLESO			1	0.929
PUNTIJARKA				1
maximum	GRIČ	MAKSIMIR	PLESO	PUNTIJARKA
GRIČ	1	0.865	0,869	0.797
MAKSIMIR		1	0.949	0.814
PLESO			1	0.841
PUNTIJARKA				1

The values of the coefficients of determination R^2 between the characteristic annual (minimum, mean, maximum) air temperature time series of four analyzed stations during the 1981-2021 period given in Table 3 indicate a strong relationship between the analyzed ATI. The highest values are determined when comparing mean annual data between stations, while the lowest values are determined when comparing the annual minimums. The strongest relationship is between stations MA

and PL (R^2=0.990) for the time series of mean annual air temperature, and the weakest is between stations PL and PU (R^2=0.472) for the time series of absolute minimum air temperature.

Figure 2a illustrates four time series of the mean annual air temperature measured at analyzed climate stations during the period 1981-2021. The linear regressions evidenced statistically significant increasing trends at all analyzed stations, which were confirmed by the results of the M–K test (i.e., p<0.01). The climate station MA has the highest value of the linear regression slope (a=0.0652 ºC/year). It is followed by the climate station GR with a value lower by 8% (a=0.0603 ºC/year). The third station is the climate station PL (a=0.0585 ºC/year). The smallest value has the climate station PU (a=0.0535 ºC/year), which is about 18% lower than the climate station MA. If we accept the assumption that at the PU climate station there is no influence of the UHI effect it seems that the highest UHI effect occurred at MA, then at GR, and then at PL.

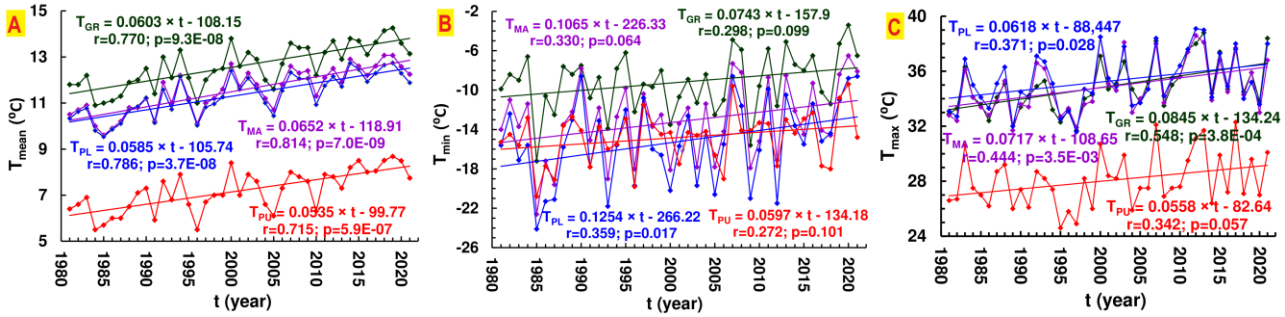

Figure 2: *Time series of the mean (a), absolute minimum (b) and absolute maximum (c) annual air temperature measured at four climate stations during the analyzed period (1981–2021). The R^2 represents the values of the coefficients of determination, and p represents the M-K test values.*

Slika 2: *Časovne vrste srednje (a), absolutne minimalne (b) in absolutne maksimalne (c) letne temperature zraka, izmerjene na štirih meteoroloških postajah v analiziranem obdobju (1981–2021). R^2 predstavlja vrednosti koeficientov determinacije, p predstavlja vrednosti preskusa M-K.*

Figure 2b illustrates four time series of the absolute minimum annual air temperature measured at the analyzed climate stations during the period 1981-2021. The linear regressions evidenced statistically insignificant increasing trends at all analyzed stations, which were corroborated by the results of the M–K test (i.e. p>0.01). Even though trends of absolute minimum air temperature series are not statistically significant, their slopes are much higher than for the time series of mean annual air temperatures. The absolute minimum air temperature increased at a faster rate than the mean annual air temperature. The linear regression slope values a are larger at all four climate stations (see Table 2). This is especially the case for PL when a_{min} (0.1254 ºC/year) is more than two times larger than a_{mean} (0.0585 ºC/year). The lowest increasing trend is at PU (a_{min}=0.0597 ºC/year). It is practically the same as the time series of mean annual air temperatures (a_{mean}=0.0535 ºC/year).

Figure 2c shows four time series of the absolute maximum annual air temperature measured at analyzed climate stations during the period 1981-2021. The linear regressions evidenced increasing trends at all analyzed stations. At GR and MA, the trends are statistically significant (i.e., p<0.01), while at PL and PU they are not statistically significant (i.e., p>0.01). The linear regression slope values at GR climate station, a_{max} (0.0845 ºC/year) are larger than for the time series of the absolute minimum annual air temperature, a_{min} (0.0743 ºC/year). At the other three stations (MA, PL, and PU), the situation is the opposite. The lowest increasing trend is at PU (a_{max}=0.0558 ºC/year). It is similar to the time series of mean annual air temperatures (a_{mean}=0.0535 ºC/year) and absolute minimum air temperature (a_{min}=0.597 ºC/year).

Analysis of the differences between ATI for all six pairs of the four analyzed climate stations during the 1981-2021 period can aid in understanding the development of UHI and DTD on increasing trends at the various analyzed parts of Zagreb. Figure 3 represents the time series of differences between mean annual air temperature (black), the absolute minimum air temperatures (blue), and the absolute maximum annual air temperature (red) for the following six pairs of the four analyzed climate stations during 1981-2021 period: (1) GR-MA (Figure 3a); (2) GR-PL (Figure 3b); (3) GR-PU (Figure 3c); (4) MA-PL (Figure 3d); (5) MA-PU (Figure 3e); (6) PL-PU (Figure 3f). The previously mentioned graphical presentation is supported by values of the time series slope a, coefficients of determination R^2, and the M–K probability p given in Table 4.

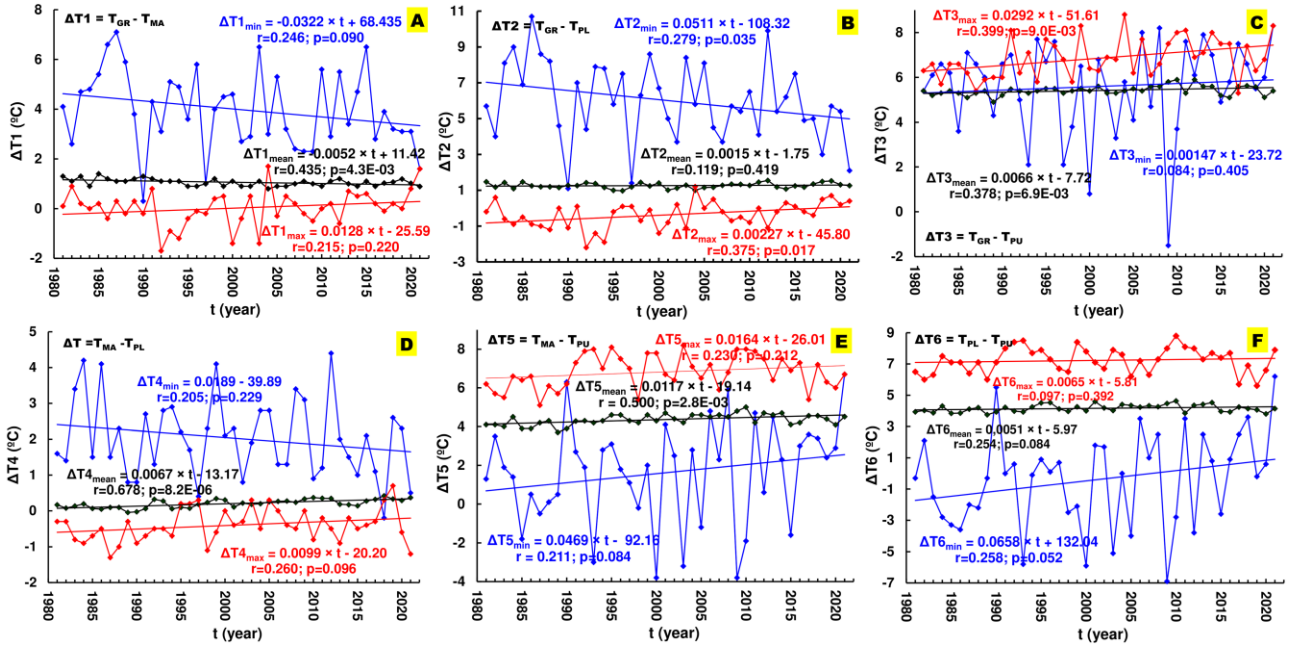

Figure 3: *Time series (1981-2021) of the differences between pairs of the mean annual air temperature (black), the absolute minimum air temperatures (blue), and the absolute maximum annual air temperature (red) for the following six pairs of the four analyzed climate stations: (1) GR-MA (Fig. 3a); (2) GR-PL (Fig. 3b); (3) GR-PU (Fig. 3c); (4) MA-PL (Fig. 3d); (5) MA-PU (Fig. 3e); (6) PL-PU (Fig. 3f). R2 represents the values of the coefficients of determination, and p represents the M-K test values.*

Slika 3*: Časovna serija (1981–2021) razlik med pari srednje letne temperature zraka (črna), absolutnih najnižjih temperatur zraka (modra) in absolutne najvišje letne temperature zraka (rdeča) za naslednjih šest parov štirih analiziranih meteoroloških postaj: (1) GR-MA (slika 3a); (2) GR-PL (slika 3b); (3) GR-PU (slika 3c); (4) MA-PL (slika 3d); (5) MA-PU (slika 3e); (6) PL-PU (slika 3f). R2 predstavlja vrednosti koeficientov determinacije, p predstavlja vrednosti preskusa M-K.*

Table 4: *Values of slope a, coefficients of determination R^2, and M–K probability p, of time series differences between annual ATI (1981–2021). M–K p values p<0.01 are highlighted in red.*

Preglednica 4*: Vrednosti naklona, a, koeficientov determinacije, R^2, in M–K verjetnosti, p, razlik časovnih vrst med letnimi ATI (1981–2021). M–K vrednosti p, p < 0,01, so označene rdeče.*

		minimum	mean	maximum
GRIČ-MAKSIMIR (Figure 3a)	a	-0.0322	-0.0052	0.0128
	R^2	0.061	0.189	0.046
	p	0.090	**4.3E-03**	0.220
GRIČ-PLESO (Figure 3b)	a	-0.0511	0.0015	0.0023
	R^2	0.078	0.014	0.141
	p	0.035	0.419	0.017
GRIČ-PUNTIJARKA (Figure 3c)	a	0.0015	0.0066	0.0292
	R^2	0.007	0.143	0.159
	p	0.405	**6.9E-03**	**9.0E-03**
MAKSIMIR-PLESO (Figure 3d)	a	-0.0189	0.0067	0.0099
	R^2	0.042	0.460	0.068
	p	0.229	**8.2E-06**	0.096
MAKSIMIR-PUNTIJARKA (Figure 3e)	a	0.0469	0.0117	0.0164
	R^2	0.045	0.250	0.053
	p	0.084	**2.8E-03**	0.212
PLESO-PUNTIJARKA (Figure 3f)	a	0.0469	0.0117	0.0164
	R^2	0.066	0.065	0.009
	p	0.084	**2.8E-03**	0.212

The differences between the absolute minimum annual air temperatures show a decline at stations MA and PL in relationship to station GR. The decreasing trend in minimum temperature differences indicates that these differences are diminishing over time, signifying that the absolute minimum annual temperature at MA increases more rapidly than at GR. The station PL shows a faster increase in absolute minimum annual temperatures than station MA. At all three urban (GR) and suburban (MA and PL) stations, the increase in the absolute minimum annual temperatures is more intensive than at the mountainous non-urban station PU. This can be explained by the fact that there is no influence of Zagreb's urban UHI effect on the PU station.

The time series of the differences between the mean annual air temperatures show a faster increasing trend (statistically significant) in suburban stations (MA) than in the town Centre (GR). It should be noted that the time series of differences between the mean annual temperature at MA and PL stations have a low increasing trend. These facts show that the MA location is more influenced by UHI than the PL location is. At all three urban (GR) and suburban (MA and PL) stations, the increase in the mean annual air temperatures is more intensive (statistically significant) than at the mountainous non-urban station PU. This can be explained by the fact that the air temperature at the station PU has no influence on UHI.

In all analyzed cases, the differences between the time series of the absolute maximum annual temperature increasing trends in city Centre (GR) are faster than in the other three locations (MA, PL, and PU). The differences between the time series of the absolute maximum annual temperature show trends in the suburban station (MA) increasing more quickly than at the airport location (PL). At all three urban (GR) and suburban (MA and PL) stations, the increase in the differences between absolute maximum annual temperatures is more intensive than at the mountainous non-urban station PU. This is a consequence of the fact that air temperature at the PU station affects only GW.

3.2 Analyses of mean monthly air temperature

Conducting monthly analyses proves valuable for assessing seasonal variations in UHI effects or the amplification of atmospheric phenomena related to air temperature caused by GW. In order to explain the adverse effects of UHI and GW and possibly take action to mitigate them, it is of particular importance to understand the behavior of mean air temperature over the course of the year. To achieve this goal, this chapter presents a trend analysis of mean monthly air temperatures at four analyzed stations for the period 1981-2021. Figure 4 shows the average values of the monthly mean air temperature (Figure 4a), minimum mean monthly air temperature (Figure 4b), maximum mean monthly air temperature (Figure 4c) and span between maximum and minimum mean monthly air temperature $Ri=T_{max.,i}-T_{min,i}$, in a month i (Figure 4d) for the time series measured at the climate stations GR (dark green), MA (purple), PL (blue), and PU (red) during the period (Jan. 1981-Dec. 2021).

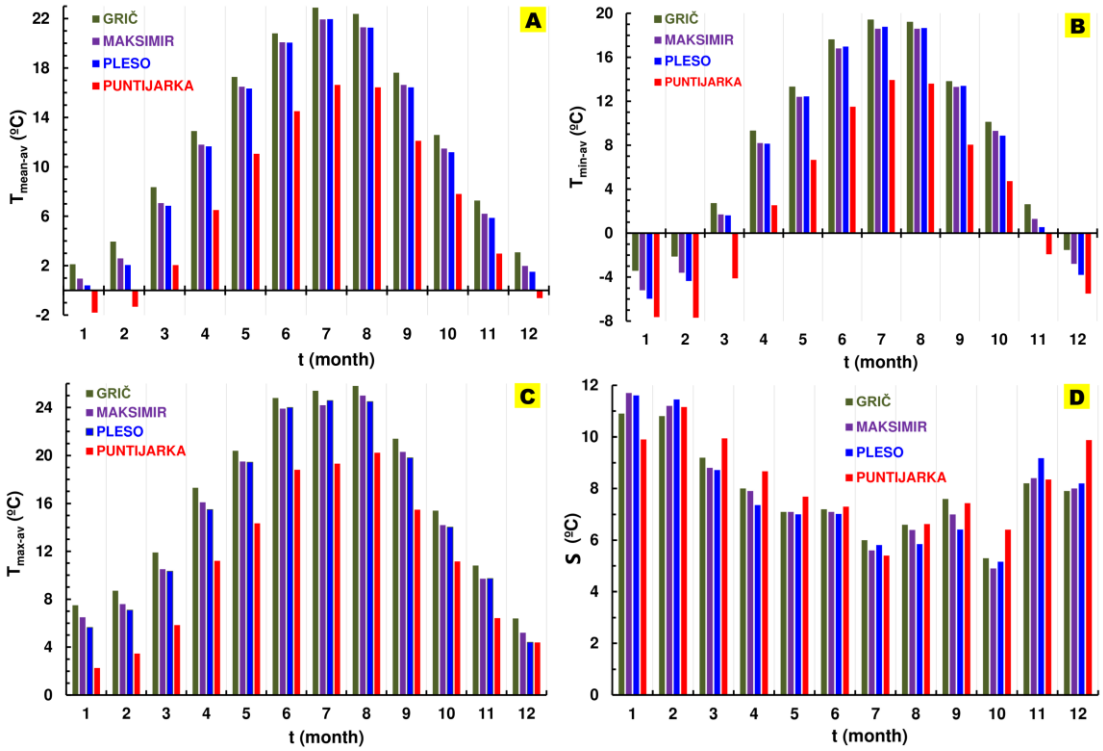

Figure 4: *The histograms of the average values of the monthly mean air temperature (Fig. 4a), absolute minimum air temperature (Fig. 4b), absolute maximum air temperature (Fig. 4c) and their span S=Tmax-Tmin, (Fig. 4d) for the time series measured at GR (dark green), MA (purple), PL (blue), and PU (red) climate stations during the period (Jan. 1981-Dec. 2021).*

Slika 4: *Histogrami povprečnih vrednosti srednje mesečne temperature zraka (slika 4a), absolutne minimalne temperature zraka (slika 4b), absolutne maksimalne temperature zraka (slika 4c) in njihov razpon, S=Tmax-Tmin, (slika 4d) za časovno vrsto, izmerjeno na meteoroloških postajah GR (temno zelena), MA (vijolična), PL (modra) in PU (rdeča) v obdobju (januar 1981–december 2021).*

The average monthly mean air temperatures in all 12 months are highest at the station GR (Figure 4a). The second is station MA, the third is PL, and the station PU has the lowest average monthly air temperature. In warm months (April-October), MA and PL stations show more similar average monthly mean air temperatures than in cold months (October-April). Only in July is the average mean air temperature at PL (21.96 ºC) slightly higher than at station MA (21.93 ºC). July is the warmest month in the mean air temperature.

Average monthly minimum air temperatures are highest in all 12 months at the GR station (Figure 4b). In January, February, May, June, July, August, September, and December the average absolute minimum air temperatures are higher at station PL than at station MA. The lowest average absolute minimum monthly air temperatures are measured at the station PU.

The average monthly maximum air temperatures are highest in all 12 months at the GR station (Figure 4c). In June, July, and November, the average absolute maximum air temperatures are higher at station PL than at station MA. The lowest average absolute maximum monthly air temperature is measured at station PU.

The behavior of the average span S is similar at all analyzed stations (Figure 4d). The lowest are in July and October, and the largest are in January and February. In general, the spans are larger in the cold (winter) than in the warm (summer) period.

Table 5 shows values of the slope of the linear regression equation a, coefficients of determination R^2, and M–K probability values p, as calculated from the time series of the mean monthly air temperatures measured at four analyzed stations during 1981-2021. Statistically significant increasing trends occurred in April, June, July, August, and November at all stations analyzed (M–K $p < 0.01$).

Table 5: *List of the slope of the linear equation a, the coefficients of determination R^2, and M–K probability values p, as calculated from the time series of the mean monthly air temperatures measured at four analyzed stations during the 1981-2021 period. M-K p values p < 0.01 are highlighted in red.*
Preglednica 5: *Seznam naklona linearne enačbe, a, koeficientov determinacije, R^2, in M–K verjetnostnih vrednosti, p, izračunanih iz časovne vrste srednjih mesečnih temperatur zraka, izmerjenih na štirih analiziranih postajah v obdobju 1981–2021. M-K vrednosti p, p < 0,01, so označene rdeče.*

month	GRIČ			MAKSIMIR			PLESO			PUNTIJARKA		
	a	R^2	p	a	R^2	p	a	R^2	p	a	R^2	p
1	0.062	0.093	0.042	0.067	0.109	0.058	0.067	0.103	0.067	0.045	0.049	0.271
2	0.092	0.136	0.023	0.100	0.160	0.011	0.104	0.161	**5.90E-03**	0.073	0.083	0.088
3	0.047	0.064	0.178	0.052	0.092	0.081	0.050	0.081	0.154	0.039	0.039	0.291
4	0.064	0.216	**6.10E-04**	0.070	0.276	**2.60E-04**	0.061	0.223	**7.50E-04**	0.072	0.224	**1.30E-03**
5	0.018	0.019	0.425	0.024	0.035	0.28	0.019	0.024	0.351	0.006	0.002	0.973
6	0.106	0.532	**1.70E-07**	0.103	0.527	**9.90E-08**	0.094	0.488	**5.10E-07**	0.093	0.436	**1.40E-06**
7	0.07	0.375	**8.30E-05**	0.075	0.440	**1.20E-05**	0.066	0.373	**9.30E-05**	0.065	0.352	**7.50E-05**
8	0.069	0.221	**4.70E-04**	0.077	0.304	**3.70E-05**	0.070	0.289	**9.30E-05**	0.068	0.209	**1.40E-03**
9	0.024	0.031	0.334	0.029	0.053	0.177	0.020	0.029	0.357	0.012	0.008	0.637
10	0.028	0.059	0.096	0.034	0.089	0.07	0.027	0.056	0.247	0.022	0.028	0.266
11	0.086	0.222	**5.30E-03**	0.095	0.268	**2.20E-03**	0.091	0.241	**4.60E-03**	0.086	0.226	**5.50E-03**
12	0.046	0.091	0.025	0.046	0.089	**9.70E-03**	0.043	0.071	0.029	0.051	0.103	0.039

Figure 5 shows histograms of values of the slope of the linear regression equation a, (Figure 5a) and the values of the coefficients of determination R^2, (Figure 5b) for the time series of mean monthly air temperature measured at the climate stations GR (dark green), MA (purple), PL (blue), and PU (red) during the period (Jan. 1981-Dec. 2021). An increasing trend was observed at all stations, in all months, and for all ATI. The behavior of the two parameters during the year is similar. The biggest increase was in June, the lowest in May (see Table 5). The reason for the different behavior in different months, especially in two adjacent months (May and June) and during the whole year, can be explained by the influence of the global circulation on the local (here analyzed) air temperature field (Pandžić, 1986; Pandžić and Kisegi, 1990). It is known that there are three main factors that generate heat patterns along the profile under consideration: (1) mainland heat, (2) sea heat, and (3) atmospheric circulation with associated cold fronts. Work is currently underway to explain this phenomenon.

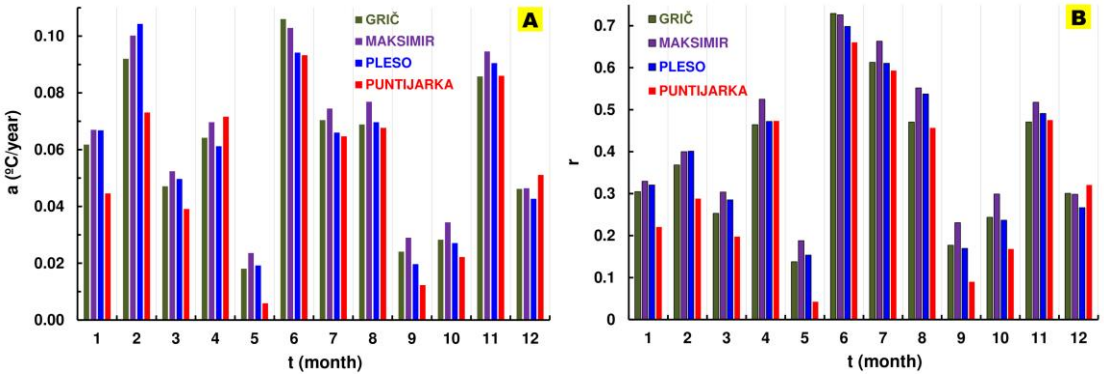

Figure 5: *Values of the slope of the linear regression equation a (Fig. 5a) and the values of the coefficients of determination R^2 (Fig. 5b) for the time series of mean monthly air temperature measured at GR (dark green), MA (purple), PL (blue), and PU (red) climate stations during the period (Jan. 1981-Dec. 2021).*

Slika 5: *Vrednosti naklona linearne regresijske enačbe, a, (slika 5a) in vrednosti koeficientov determinacije, R^2, (slika 5b) za časovno vrsto srednje mesečne temperature zraka, izmerjene na meteoroloških postajah GR (temnozelena), MA (vijolična), PL (modra) in PU (rdeča) v obravnavanem obdobju (januar 1981–december 2021).*

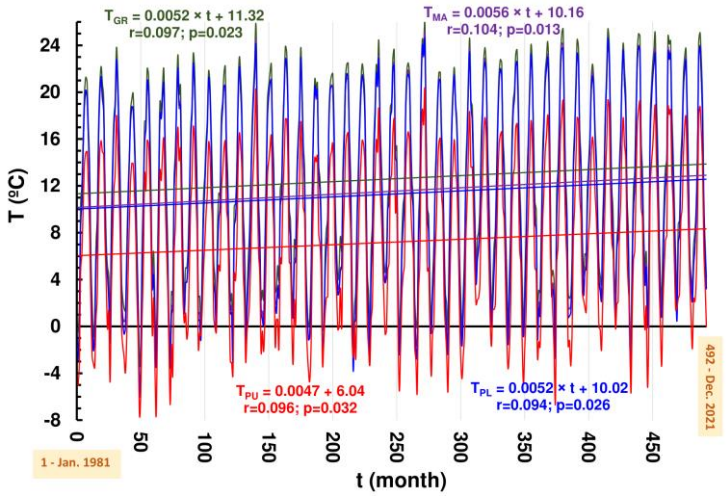

Figure 6: *Time series of the mean monthly air temperature measured at four climate stations during the analyzed period (Jan. 1981-Dec. 2021; 492 months in total). R^2 represents the values of the coefficients of determination, and p represents the M–K test values.*

Slika 6: *Časovna vrsta srednje mesečne temperature zraka, izmerjene na štirih meteoroloških postajah v analiziranem obdobju (jan. 1981–dec. 2021; skupaj 492 mesecev). R^2 predstavlja vrednosti koeficientov determinacije, p pa predstavlja vrednosti preskusa M–K.*

A graphical representation of four time series of the mean monthly air temperature measured at four climate stations during the analyzed period (Jan. 1981-Dec. 2021, total 492 months) is shown in Figure 6. The trend is upward for climate stations. The values of the slope of the linear regression equations, a, are as follows: (1) MA (a=0.0056 ºC/year); (2) GR (a=0.00522 ºC/year); (3) PL (a=0.0052 ºC/year); (4) PU (a=0.0047 ºC/year).

3.3 DTD

Equations (3) and (4) were used to calculate the annual values (1 January to 31 December) $DTDT_{min}$, $DTDT_{mean}$, $DTDT_{max}$, and ΔDTD individually for each year for the period from 1981 to 2021 (41 years in total). Due to the war in 1990, the station PL was not in operation for a few days. The same happened in 2000 due to an earthquake. Due to incomplete daily measurements, the DTD variations in air temperature were not calculated for these two stations in these two years. Table 6 lists the following characteristics for each of the four-time series from DTD and for all climate stations analyzed: (1) minimum, (2) average, (3) maximum, (4) span.

Table 6: *Characteristic values (minimum, average, maximum, span) of $DTDT_{min}$, $DTDT_{mean}$, $DTDT_{max}$, and ΔDTD for the whole year for four analyzed climate stations.*

Preglednica 6: *Značilne vrednosti (minimum, povprečje, maksimum, razpon) $DTDT_{min}$, $DTDT_{mean}$, $DTDT_{max}$, ΔDTD, za celo leto za štiri analizirane meteorološke postaje.*

		$DTDT_{min}$	$DTDT_{mean}$	$DTDT_{max}$	ΔDTD
GRIČ	minimum	1.543	1.575	2.068	0.251
	average	1.783	1.802	2.254	0.471
	maximum	2.014	2.031	2.463	0.648
	span	0.471	0.456	0.395	0.397
MAKSIMIR	minimum	1.727	1.574	2.226	-0.023
	average	2.218	1.941	2.476	0.258
	maximum	2.544	2.198	2.698	0.610
	span	0.817	0.624	0.472	0.633
PLESO	minimum	1.844	1.545	2.295	0.054
	average	2.251	1.853	2.560	0.309
	maximum	2.543	2.134	2.190	0.618
	span	0.699	0.589	0.615	0.564
PUNTIJARKA	minimum	1.614	1.776	2.136	0.241
	average	1.919	2.095	2.435	0.515
	maximum	2.206	2.383	2.669	0.898
	span	0.592	0.606	0.533	0.657

Table 7: *List of the slope of the linear equation a, the coefficients of determination R^2, and M–K probability values p, as calculated from the time series of the DTD_{min}, DTD_{mean}, DTD_{max}, and ΔDTD at four analyzed stations during the 1 Jan 1981- 31 Dec. 2021 period. M–K p values p < 0.01 are highlighted in red.*

Preglednica 7: *Seznam naklona linearne enačbe, a, koeficientov determinacije, R^2, in vrednosti verjetnosti M–K, p, izračunanih iz časovne vrste DTD_{min}, DTD_{mean}, DTD_{max} in ΔDTD, na štirih analiziranih postajah med 1. jan. 1981 in 31. dec. 2021. Vrednosti M–K p, p < 0,01, so označene rdeče.*

		R2	a	p
$DTDT_{min}$	GRIČ	0.035	-0.0018	0.196
	MAKSIMIR	0.054	-0.003	0.351
	PLESO	0.049	-0.003	0.311
	PUNTIJARKA	0.011	-0.0013	0..351
$DTDT_{mean}$	GRIČ	0.054	-0.0021	0.139
	MAKSIMIR	0.078	-0.0031	0.090
	PLESO	0.041	-0.0022	0.173
	PUNTIJARKA	0.154	-0.005	0.021
$DTDT_{max}$	GRIČ	0.003	-0.0005	0.600
	MAKSIMIR	0.006	-0.0008	0.438
	PLESO	0.070	-0.0027	0.180
	PUNTIJARKA	0.175	-0.005	**8.7E-03**
ΔDTD	GRIČ	0.024	0.0013	0.408
	MAKSIMIR	0.039	0.0024	0.438
	PLESO	0.0005	0.0003	0.789
	PUNTIJARKA	0.106	-0.0037	0.052

Table 7 is the matrix of values of the slope of the linear equation a, the coefficients of determination R2, and M–K probability values p, as calculated from the time series of the $DTDT_{min}$, $DTDT_{mean}$, $DTDT_{max}$, and ΔDTD at four analyzed stations during the period from 1 January 1981 to 31 December 2021.

Figure 7a shows the graphical representation of the time series of annual values (1 January to 31 December) of $DTDT_{mean}$ at four analyzed climate stations in the period 1981–2021 with plotted linear trend lines, the coefficients of determination R^2, and the results of the M–K test p. A statistically insignificant decreasing trend occurred at all analyzed climate stations. The strongest decreasing trend occurred at PU station, while at other urban and suburban points it is similar. At the GR station, the $DTDT_{mean}$ average value is the lowest (1.802 ºC), at PL it is 0.051 ºC (1.853 ºC) higher, at MA it is 0.109 ºC (1.941 ºC) higher, and at PU it is highest (2.095 ºC), i.e. 0.242 ºC higher than at GR.

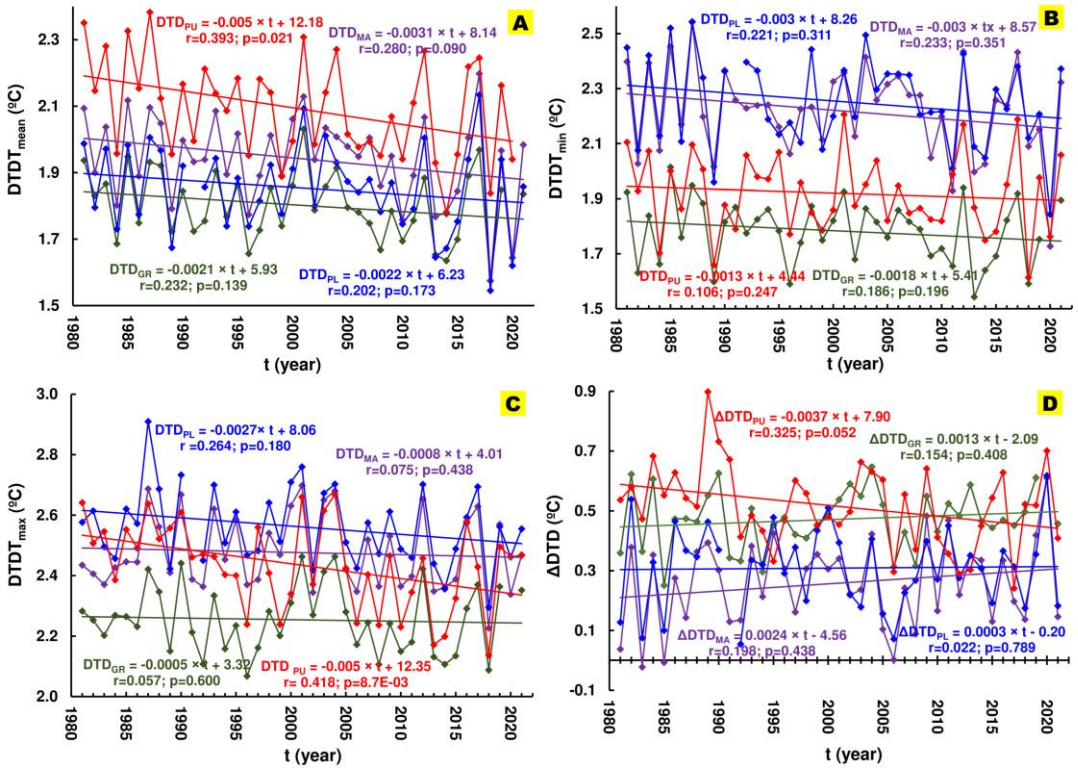

Figure 7: *Time series of annual values (1 Jan.-31 Dec.) of DTD_{mean} (Fig. 7a), DTD_{min} (Fig. 7b), DTD_{max} (Fig. 7c) and $\Delta DTD=DTD_{max}-DTD_{min}$ (Fig. 7d) at four analyzed climate stations, during the 1981–2021 period with designated linear trend lines, coefficients of determination R^2, and the results of the M–K test, p.*

Slika 7: *Časovna vrsta letnih vrednosti (1. januar–31. december) DTD_{mean} (slika 7a), DTD_{min} (slika 7b), DTD_{max} (slika 7c) in $\Delta DTD=DTD_{max}-DTD_{min}$ (slika 7d) pri štirih analiziranih meteoroloških postajah, v obdobju 1981–2021 z označenimi linearnimi trendnimi črtami, koeficienti determinacije R^2 in rezultati preskusa M–K, p.*

Figure 7b shows the graphical representation of the time series of annual values (1 January – 31 December) of $DTDT_{min}$ at four analyzed climate stations, in the period 1981–2021 with plotted linear trend lines, the coefficients of determination R^2, and the results of the M–K test p. A statistically insignificant decreasing trend occurred at all analyzed climate stations. The least is at the PU station, while at other urban and suburban points it is similar. At the GR station, the $DTDT_{min}$ average value is the lowest (1.783 ºC), at PU it is 0.163 ºC higher, at MA it is 0.435 ºC higher, and at PL it is highest, i.e. 0.468 ºC higher than at GR.

Figure 7c shows the graphical representation of the time series of annual values (1 January – 31 December) of DTD_{max} at four analyzed climate stations in the period 1981–2021, with plotted linear trend lines, the coefficients of determination R^2, and the results of the M–K test p. A statistically significant decreasing trend occurred only at the PU station, while at other three analyzed climate stations the trends were statistically insignificant. The greatest was at the PU station, while at other urban and suburban points it is similar. At the GR station, the DTD_{max} average value is the lowest (2.254 ºC), at PU it is 0.181 ºC higher, at MA it is 0.222 ºC higher, and at PL it is highest (2.560 ºC), i.e. 0.306 ºC higher than at GR.

The lowest average values of all three discussed DTD indices at four analyzed stations were found at station GR. Most likely, this is related to the strongest UHI and GW processes occurring in the city Centre.

Figure 7d shows the graphical representation of the time series of annual values (1 January – 31 December) of ΔDTD at four analyzed climate stations in the period 1981–2021, with plotted linear trend lines, the coefficients of determination R^2, and

the results of the M–K test p. A statistically insignificant decreasing trend occurred at the PU station, while at others there was a statistically insignificant increasing trend. At the MA station, the ΔDTD average value is the lowest (0.258 ºC), at PL it is 0.051 ºC (0.309 ºC) higher, at GR it is 0.113 ºC (0.471 ºC) higher, and at PU is highest (0.515 ºC), i.e., 0.257 ºC higher than at GR.

The values of ΔDTD at all analyzed stations are generally positive (with the exception of two years at MA), suggesting that variations in air temperature during the night are smaller than during the day because nighttime temperatures are attenuated by the effect of UHI (Gough, 2008; Gough and Hu, 2016; Tam et al., 2015; Tam and Gough, 2012).

3.4 DTR

Figure 8 represents the time series of annual values of DTR at four analyzed climate stations in the period 1981–2021, with plotted linear trend lines, the coefficients of determination R^2, and the results of the M–K test p. A statistically significant increasing trend occurred only at the GR station. A statistically insignificant increasing trend occurs at the PL station, while there are statistically insignificant decreasing trends at the other two analyzed climate stations (MA and PU). The greatest is at the GR station. At the PU station, the DTR average value is the lowest (6.62 ºC), at GR it is 1.30 ºC higher, at MA it is 3.28 ºC higher, and at PL it is the highest (10.54 ºC), i.e. 3.92 ºC higher than at PU.

It is worth highlighting the very different behavior of trends and different DTR values in the city center (the strong increasing trend at GR), at the mountain station (the strong decreasing trend at PU), and practically no trends and high DTR values at the two suburban stations (MA and PL).

To clarify the impact of solar and thermal surface radiation on global warming, Wild et al. (2007) focused on the daily temperature cycle using DTR. They concluded that global dimming masked global warming until the 1980s, but that the subsequent era of global brightening revealed the full impact of greenhouse gases and led to accelerated temperature increases.

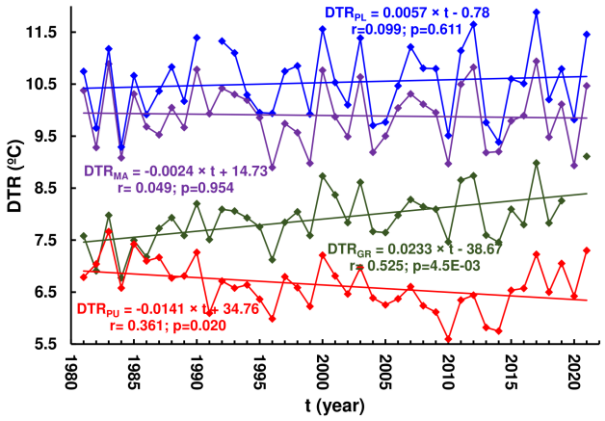

Figure 8. *Time series of annual values of DR at four analyzed climate stations, during the 1981–2021 period with designated linear trend lines, coefficients of determination, R^2, and the results of the M–K test, p.*

Slika 8: *Časovne vrste letnih vrednosti DR na štirih analiziranih meteoroloških postajah, v obdobju 1981–2021 z označenimi linearnimi trendnimi črtami, koeficienti determinacije R^2 in rezultati preskusa M–KM–K, p.*

Vose et al. (2005) confirm the conclusions of Easterling et al. (1997) that the minimum temperature increased at a faster rate than the maximum temperature during the latter half of the 20th century, resulting in a significant decrease in the DTR for this period. In contrast, increases in maximum and minimum temperatures during the satellite era were roughly comparable, dampening recent changes in DTR. The maximum and minimum temperatures increased in both periods in almost all parts of the globe, while a widespread decrease in DTR was observed only from 1950 to 1980.

The global decrease in DTR is attributed to an anthropogenic signal caused primarily by greenhouse gas forcing (Liu et al., 2022). Liu et al. (2022) emphasized that the decline in global DTR and its impact on human and natural systems have been widely reported. It remains unclear as to whether humans have a detectable impact on DTR and to what extent anthropogenic greenhouse gases can cause such changes. The results reported in this paper show different behavior of DTR at different sites.

4. Conclusions and recommendation for further investigation

The occurrence and intensity of trends in the two analyzed indices, DTD and DTR, are simultaneously influenced by global warming and UHI. Without more accurate and long-term measurements of climatological, urban, ecological (especially vegetation and soil), geographic, and other data, it is very difficult to reliably determine how and to what extent each of these factors affects ambient temperatures. DTD responds faster and more vigorously to global warming stimuli, while DTR is more strongly influenced by local UHI factors such as warming (during winter), cooling (during summer heat), the presence and development of vegetation cover, etc. Unfortunately, these assumptions cannot be proven at this stage, and it will most likely be necessary to develop a complex model based on detailed monitoring of the possible factors.

Analyzing the annual mean urban-rural temperature differences, and rural temperatures in American, Argentinean, and Australian cities, Camilloni and Barros (1997) found that they are negatively correlated in almost all cases, suggesting that the intensity of the urban heat island depends on temperature itself, in addition to other parameters. They concluded that this negative correlation is related to the fact that the interannual variability of temperature in urban environments is generally lower than in rural areas.

In estimating the environmental footprint of the heat island effect over Athens (Greece), Santamouris et al. (2007) point out that the major energy problems caused by the UHI effect are related to the substantial increase in energy consumption for cooling purposes and the substantial increase in peak electricity load.

To better understand and explain the different behaviors of UHIs and GW in a relatively small urban and suburban area (about 200 km^2), three different methods (trend analysis, DTD, DTR) were used in this work. Each of them indicates different aspects of UHI and/or GW. By comparing the intensity of the temperature increase at urban stations such as Grič and Maksimir with those having a lower level of urbanization, such as Puntijarka, the rough estimate is that UHI is responsible for about 10% of the increase in air temperature in the urban center (GR) and suburban areas influenced by intensive urbanization (MA). The strongest increasing trend of air temperature at the suburban station MA is due to intensive urbanization in recent decades.

Since each city or district has specific natural and man-made features that have more or less influence on the UHI and/or GW process, it is crucial to capture and explain them in detail. Each case requires individual solutions. For this reason, a variety of information and data should be available. The problem, however, is that such data are usually lacking. To mitigate the negative effects of increasing UHI and GW in urban areas, long-term, well-organized, and continuous interdisciplinary actions should be taken. The case of the four climate stations in and around the city of Zagreb discussed in this article strongly confirms the previous statement. It should also be emphasized that recognizing the significant influence of urban heat islands on water availability underscores the necessity for implementing comprehensive urban water management strategies aimed at mitigating the adverse effects of accelerated evaporation and altered precipitation patterns in urban environments.

Funding

This research was supported through the project KK.05.1.1.02.0024 "VODIME-Waters of Imotski Region," a project financed by the Croatian Government and the European Union through the European Structural Fund – within the call "Strengthening the applied research for climate change adaptation measures" KK.05.1.1.02.380.

This research is partially supported through the project KK.01.1.1.02.0027, a project co-financed by the Croatian Government and the European Union through the European Regional Development Fund – the Competitiveness and Cohesion Operational Programme.

Author contributions

Conceptualization, data curation, formal analysis, investigation and writing - original draft preparation, O.B.; writing - review and editing, A.V, data curation, formal analysis, T.R.B. All authors have read and agreed to the published version of the manuscript.

References

Alcoforado, M.J., Andrade, H. (2008). Global Warming and the Urban Heat Island, in: Urban Ecology. Springer US, Boston, MA, pp. 249–262. https://doi.org/10.1007/978-0-387-73412-5_14.

Allegrini, J., Carmeliet, J. (2018). Simulations of local heat islands in Zürich with coupled CFD and building energy models. *Urban Clim* **24**, 340–359. https://doi.org/10.1016/j.uclim.2017.02.003.

Antoszewski, P., Krzyżaniak, M., Świerk, D. (2022). The Future of Climate-Resilient and Climate-Neutral City in the Temperate Climate Zone. *Int J Environ Res Public Health* **19**, 4365. https://doi.org/10.3390/ijerph19074365.

Bonacci, O., Andrić, I., Roje-Bonacci, T. (2018). Increasing trends of air temperature in urban area: a case study from four stations in Zagreb city area. *Vodoprivreda* 50, 203–214.

Bonacci, O., Roje Bonacci, T. (2018). Analyses of the Zagreb Grič observatory air temperatures indices for the period 1881 to 2017. *Acta hydrotechnica*. https://doi.org/10.15292/acta.hydro.2018.05.

Bonacci, O., Roje-Bonacci, T., Vrsalović, A. (2022). The day-to-day temperature variability method as a tool for urban heat island analysis: A case of Zagreb-Grič Observatory (1887–2018). *Urban Clim* **45**, 101281. https://doi.org/10.1016/j.uclim.2022.101281.

Brzoja, D. (2012). Analysis of occurrence of fogin the wider Zagreb region. University of Zagreb, Zagreb.

Camilloni, I., Barros, V. (1997). On the Urban Heat Island effect dependence on temperature trends. *Clim Change* **37**, 665–681. https://doi.org/10.1023/A:1005341523032.

Cekinir, S., Ozgener, O., Ozgener, L. (2022). A study on heating and cooling requirements for green buildings and refugee settlements. *International Journal of Global Warming* **26**, 391. https://doi.org/10.1504/IJGW.2022.122432.

Clay, R., Guan, H., Wild, N., Bennett, J., Vinodkumar, Ewenz, C. (2016). Urban Heat Island traverses in the City of Adelaide, South Australia. *Urban Clim* **17**, 89–101. https://doi.org/10.1016/j.uclim.2016.06.001.

de Munck, C., Pigeon, G., Masson, V., Meunier, F., Bousquet, P., Tréméac, B., Merchat, M., Poeuf, P., Marchadier, C. (2013). How much can air conditioning increase air temperatures for a city like Paris, France? *International Journal of Climatology* **33**, 210–227. https://doi.org/10.1002/joc.3415.

Deluka-Tibljaš, A., Cuculić, M., Šurdonja, S., Babić, S. (2012). Analysis of pavement surface heating in urban areas. Journal of the Croatian *Association of Civil Engineers* **64**, 127–134. https://doi.org/10.14256/JCE.641.2011.

Easterling, D.R., Horton, B., Jones, P.D., Peterson, T.C., Karl, T.R., Parker, D.E., Salinger, M.J., Razuvayev, V., Plummer, N., Jamason, P., Folland, C.K. (1997). Maximum and Minimum Temperature Trends for the Globe. *Science* (1979) **277**, 364–367. https://doi.org/10.1126/science.277.5324.364.

Giridharan, R., Kolokotroni, M. (2009). Urban heat island characteristics in London during winter. *Solar Energy* **83**, 1668–1682. https://doi.org/10.1016/j.solener.2009.06.007.

Gonzalez-Trevizo, M.E., Martinez-Torres, K.E., Armendariz-Lopez, J.F., Santamouris, M., Bojorquez-Morales, G., Luna-Leon, A. (2021). Research trends on environmental, energy and vulnerability impacts of Urban Heat Islands: An overview. *Energy Build* **246**, 111051. https://doi.org/10.1016/j.enbuild.2021.111051.

Gough, W.A. (2008). Theoretical considerations of day-to-day temperature variability applied to Toronto and Calgary, Canada data. *Theor Appl Climatol* **94**. https://doi.org/10.1007/s00704-007-0346-9.

Gough, W.A., Hu, Y. (2016). Day-to-day temperature variability for four urban areas in

China. *Urban Clim* **17**. https://doi.org/10.1016/j.uclim.2016.06.002.

Gough, W.A., Leung, A.C.W. (2022). Do Airports Have Their Own Climate? *Meteorology* **1**, 171–182. https://doi.org/10.3390/meteorology1020012.

Gough, W.A., Shi, B. (2020). Impact of Coastalization on Day-to-Day Temperature Variability along China's East Coast. *J Coast Res* **36**. https://doi.org/10.2112/JCOASTRES-D-19-00167.1.

He, B.-J., Wang, J., Zhu, J., Qi, J. (2022). Beating the urban heat: Situation, background, impacts and the way forward in China. *Renewable and Sustainable Energy Reviews* **161**, 112350. https://doi.org/10.1016/j.rser.2022.112350.

Hussain, Md., Mahmud, I. (2019). pyMannKendall: a python package for non parametric Mann Kendall family of trend tests. *J Open Source Softw* **4**, 1556. https://doi.org/10.21105/joss.01556

Karl, T.R., Kukla, G., Gavin, J. (1987). Recent Temperature Changes during Overcast and Clear Skies in the United States. *Journal of Climate and Applied Meteorology* **26**, 698–711. https://doi.org/10.1175/1520-0450(1987)026<0698:RTCDOA>2.0.CO;2.

Karl, T.R., Kukla, G., Gavin, J. (1984). Decreasing Diurnal Temperature Range in the United States and Canada from 1941 through 1980. *Journal of Climate and Applied Meteorology* **23**, 1489–1504. https://doi.org/10.1175/1520-0450(1984)023<1489:DDTRIT>2.0.CO;2.

Klaić, Z.B., Nitis, T., Kos, I., Moussiopoulos, N. (2002). Modification of the local winds due to hypothetical urbanization of the Zagreb surroundings. *Meteorology and Atmospheric Physics* **79**, 1–12. https://doi.org/10.1007/s703-002-8225-z.

Kolokotroni, M., Giannitsaris, I., Watkins, R. (2006). The effect of the London urban heat island on building summer cooling demand and night ventilation strategies. *Solar Energy* **80**, 383–392. https://doi.org/10.1016/j.solener.2005.03.010.

L. El Zein, A. (2015). The Effect of Greenhouse Gases on Earth's Temperature. International *Journal of Environmental Monitoring and Analysis* **3**, 74. https://doi.org/10.11648/j.ijema.20150302.16.

Lemoine-Rodríguez, R., Inostroza, L., Zepp, H. (2022). Does urban climate follow urban form? Analysing intraurban LST trajectories versus urban form trends in 3 cities with different background climates. *Science of The Total Environment* **830**, 154570. https://doi.org/10.1016/j.scitotenv.2022.154570.

Li, J., Song, C., Cao, L., Zhu, F., Meng, X., Wu, J. (2011). Impacts of landscape structure on surface urban heat islands: A case study of Shanghai, China. *Remote Sens Environ* **115**, 3249–3263. https://doi.org/10.1016/j.rse.2011.07.008.

Liang, Z., Wu, S., Wang, Y., Wei, F., Huang, J., Shen, J., Li, S. (2020). The relationship between urban form and heat island intensity along the urban development gradients. *Science of The Total Environment* **708**, 135011. https://doi.org/10.1016/j.scitotenv.2019.135011.

Likso, T. (2003). Inhomogeneities in temperature time series in Croatia. *Hrvatski Meteorološki Časopis* **38**, 3–9.

Liu, J., Feng, X., Gu, X., Zhang, J., Slater, L.J., Kong, D. (2022). Detection and Attribution of Human Influence on the Global Diurnal Temperature Range Decline. *Geophys Res Lett* **49**. https://doi.org/10.1029/2021GL097155.

Louiza, H., Zéroual, A., Djamel, H. (2015). Impact of the transport on the urban heat island. International *Journal for Traffic and Transport Engineering* **5**, 252–263. https://doi.org/10.7708/ijtte.2015.5(3).03.

Lu, Y., Yue, W., He, T., Shan, Z. (2022). Urban form centrality and thermal environment: An empirical study of Chinese megacities. *Sustain Cities Soc* **83**, 103955. https://doi.org/10.1016/j.scs.2022.103955.

Meng, Q., Hu, D., Zhang, Y., Chen, X., Zhang, L., Wang, Z. (2022). Do industrial parks generate intra-heat island effects in cities? New evidence, quantitative methods, and contributing factors from a spatiotemporal analysis of top steel plants in China. *Environmental Pollution* **292**, 118383. https://doi.org/10.1016/j.envpol.2021.118383.

Milošević, D., Trbić, G., Savić, S., Popov, T., Ivanišević, M., Marković, M., Ostojić, M., Dunjić, J., Fekete, R., Garić, B. (2022=. Biometeorological conditions during hot summer days in diverse urban environments of Banja Luka (Bosnia and Herzegovina). *Geographica Pannonica* **26**, 29–45. https://doi.org/10.5937/gp26-35456.

Moberg, A., Jones, P.D., Barriendos, M., Bergström, H., Camuffo, D., Cocheo, C., Davies, T.D., Demarée, G., Martin-Vide, J., Maugeri, M.,

Rodriguez, R., Verhoeve, T. (2000). Day-to-day temperature variability trends in 160- to 275-year-long European instrumental records. *Journal of Geophysical Research: Atmospheres* **105**, 22849–22868. https://doi.org/10.1029/2000JD900300.

Nimac, I., Herceg-Bulić, I., Cindrić Kalin, K., Perčec Tadić, M. (2021). Changes in extreme air temperatures in the mid-sized European city situated on southern base of a mountain (Zagreb, Croatia). *Theor Appl Climatol* **146**, 429–441. https://doi.org/10.1007/s00704-021-03689-8.

Nitis, T., Klaić B., Z., Moussiopoulos, N. (2005). Effects of Topography on the Urban Heat Island, in: 10th Conference on Harmonisation within Atmospheric Dispersion Modelling for Regulatory Purposes. Sissi, Crete, Greece.

Nuruzzaman, Md. (2015). Urban Heat Island: Causes, Effects and Mitigation Measures – A Review. *International Journal of Environmental Monitoring and Analysis* **3**. https://doi.org/10.11648/j.ijema.20150302.15.

Oke, T.R. (1982). The energetic basis of the urban heat island. *Quarterly Journal of the Royal Meteorological Society* **108**. https://doi.org/10.1002/qj.49710845502.

Pandžić, K. (1986=. Factor analysis of temperature field on a relatively small area. *Idojaras* **90**, 321–331.

Pandžić, K., Kisegi, M. (1990=. Principal Component analysis of a local temperature field within the global circulation. *Theor Appl Climatol* **41**, 177–200. https://doi.org/10.1007/BF00866450.

Park, H.S., Joh, M. (2005). Climate Change due to the Gradual Increase in Atmospheric CO₂: A Climate System Model Sensitivity Study. *Key Eng Mater* 277–279, 595–600. https://doi.org/10.4028/www.scientific.net/KEM.277-279.595.

Peterson, T.C. (2003). Assessment of Urban Versus Rural In Situ Surface Temperatures in the Contiguous United States: No Difference Found. *J Clim* **16**, 2941–2959. https://doi.org/10.1175/1520-0442(2003)016<2941:AOUVRI>2.0.CO;2.

Qu, M., Wan, J., Hao, X. (2014). Analysis of diurnal air temperature range change in the continental United States. *Weather Clim Extrem* **4**, 86–95. https://doi.org/10.1016/j.wace.2014.05.002.

Raupach, M., Fraser, P. (2011=. Climate and greenhouse gases, in: Climate Changes: ….

Santamouris, M. (2014). Cooling the cities – A review of reflective and green roof mitigation technologies to fight heat island and improve comfort in urban environments. *Solar Energy* **103**. https://doi.org/10.1016/j.solener.2012.07.003.

Santamouris, M., Paraponiaris, K., Mihalakakou, G. (2007). Estimating the ecological footprint of the heat island effect over Athens, Greece. *Clim Change* **80**, 265–276. https://doi.org/10.1007/s10584-006-9128-0.

Seletković, A., Kičić, M., Ančić, M., Kolić, J., Pernar, R. (2023). The Urban Heat Island Analysis for the City of Zagreb in the Period 2013–2022 Utilizing Landsat 8 Satellite Imagery. *Sustainability* **15**, 3963. https://doi.org/10.3390/su15053963.

Seletković, I., Potočić, N., Ugarković, D., Jazbec, A., Pernar, R., Seletković, A., Benko, M. (2009). Climate and relief properties influence crown condition of common beech (Fagus sylvatica L.) on the Medvednica massif. Period Biol 111.

Stocker, T.F., D. Qin, G.-K., Plattner, M.T., Allen, S.K., Boschung, J., Nauels, A., Xia, Y., Bex, V., Midgley, P.M., 2013. IPCC, 2013: Summary for Policymakers. In: Climate Change 2013: The Physical Science Basis. Contribution of Working Group I to the Fifth Assessment Report of the IPCC, Cambridge University Press. Cambridge, United Kingdom and New York, NY, USA.

Takebayashi, H., Senoo, M. (2018). Analysis of the relationship between urban size and heat island intensity using WRF model. *Urban Clim* **24**, 287–298. https://doi.org/10.1016/j.uclim.2016.12.003.

Tam, B.Y., Gough, W.A. (2012). Examining past temperature variability in Moosonee, Thunder Bay, and Toronto, Ontario, Canada through a day-to-day variability framework. *Theor Appl Climatol* **110**. https://doi.org/10.1007/s00704-012-0622-1.

Tam, B.Y., Gough, W.A., Mohsin, T. (2015). The impact of urbanization and the urban heat island effect on day to day temperature variation. *Urban Clim* **12**. https://doi.org/10.1016/j.uclim.2014.12.004.

Vose, R.S., Easterling, D.R., Gleason, B. (2005). Maximum and minimum temperature trends for the globe: An update through 2004. *Geophys Res Lett*

32, L23822. https://doi.org/10.1029/2005GL024379.

Wild, M., Ohmura, A., Makowski, K. (2007). Impact of global dimming and brightening on global warming. *Geophys Res Lett* **34**, L04702. https://doi.org/10.1029/2006GL028031.

Zoldoš, M., Jurkovic, J. (2016). Fog event climatology for Zagreb Airport. *Hrvatski Meteoroloski Casopis* **51**, 13–26.